

Opposite Shear Senses: a comprehensive review of geneses, global occurrences, and a case study



Dripta Dutta*



Soumyajit Mukherjee

Geodynamics Lab, Department of Earth Sciences
Indian Institute of Technology Bombay.

*e-mail: dripta.dutta@gmail.com



1. Background

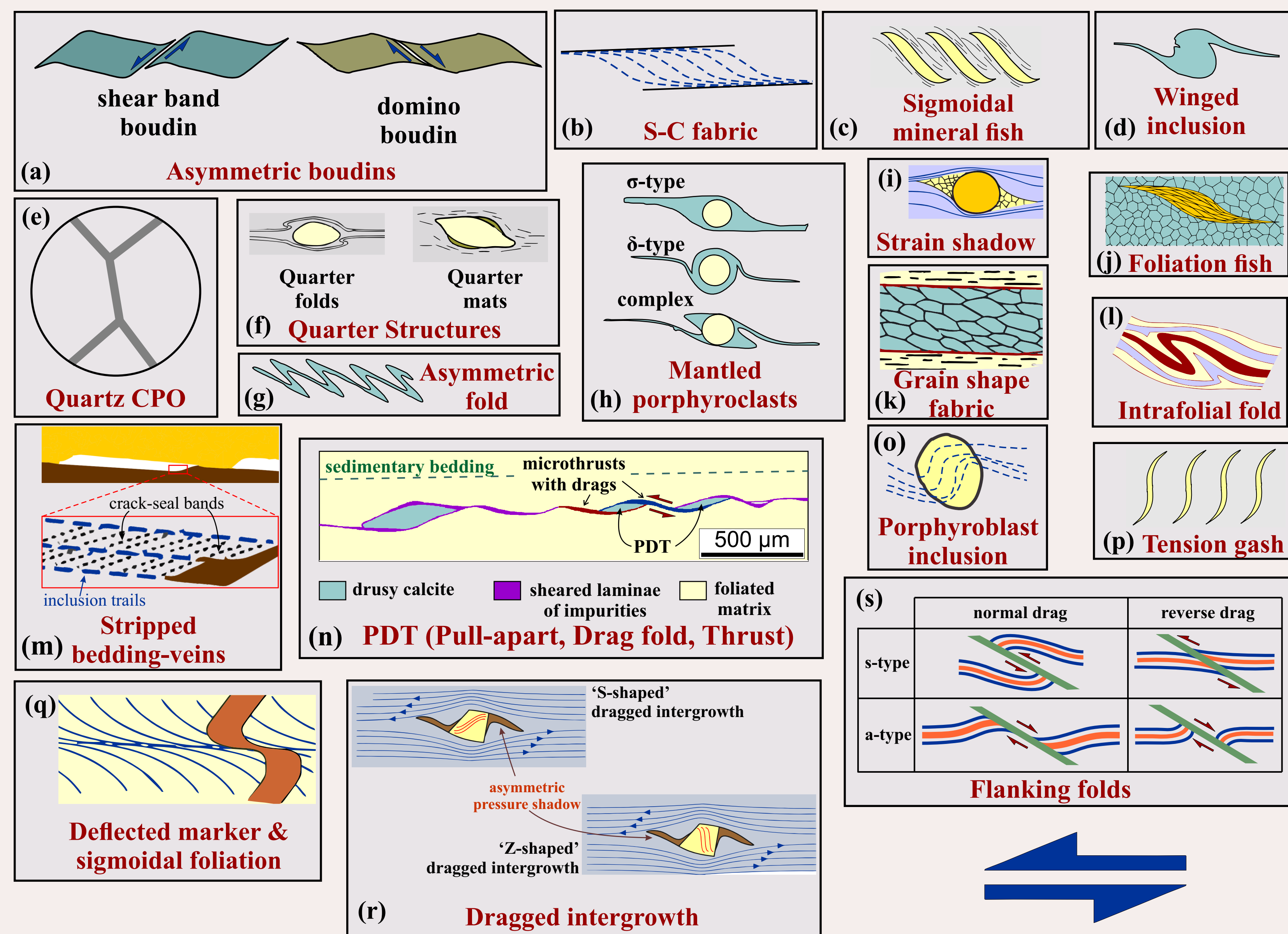


Fig. 1. Major ductile shear sense indicators observed at meso- and micro-scale. Reproduced from (a) fig. 5c of Goscombe et al. (2004), fig. 4c of Grasmann et al. (2019), (d) fig. 2 of Driessche & Brun (1987), (f) fig. 5.38 of Passchier & Trouw (2005), (h) fig. 5.21 of Passchier & Trouw (2005), (i) fig. 9.7.13 of Trouw et al. (2010), (j) fig. 9.5.2 of Trouw et al. (2010), (k) fig. 10a of Xypolias (2010), (l) fig. 12.2c of Mukherjee et al. (2015) (m) fig. 10a of Koehn & Passchier (2000), (n,r) figs. 9 & 11d of Scharf et al. (2019), (o) fig. 5.73 of Vernon (2004), (p) fig. 8a of Fossen & Cavalcante (2017), (q) fig. 9.1 of Trouw et al. (2010), (s) fig. 1 of Grasmann et al. (2003). Shear sense: sinistral (blue half-arrows).

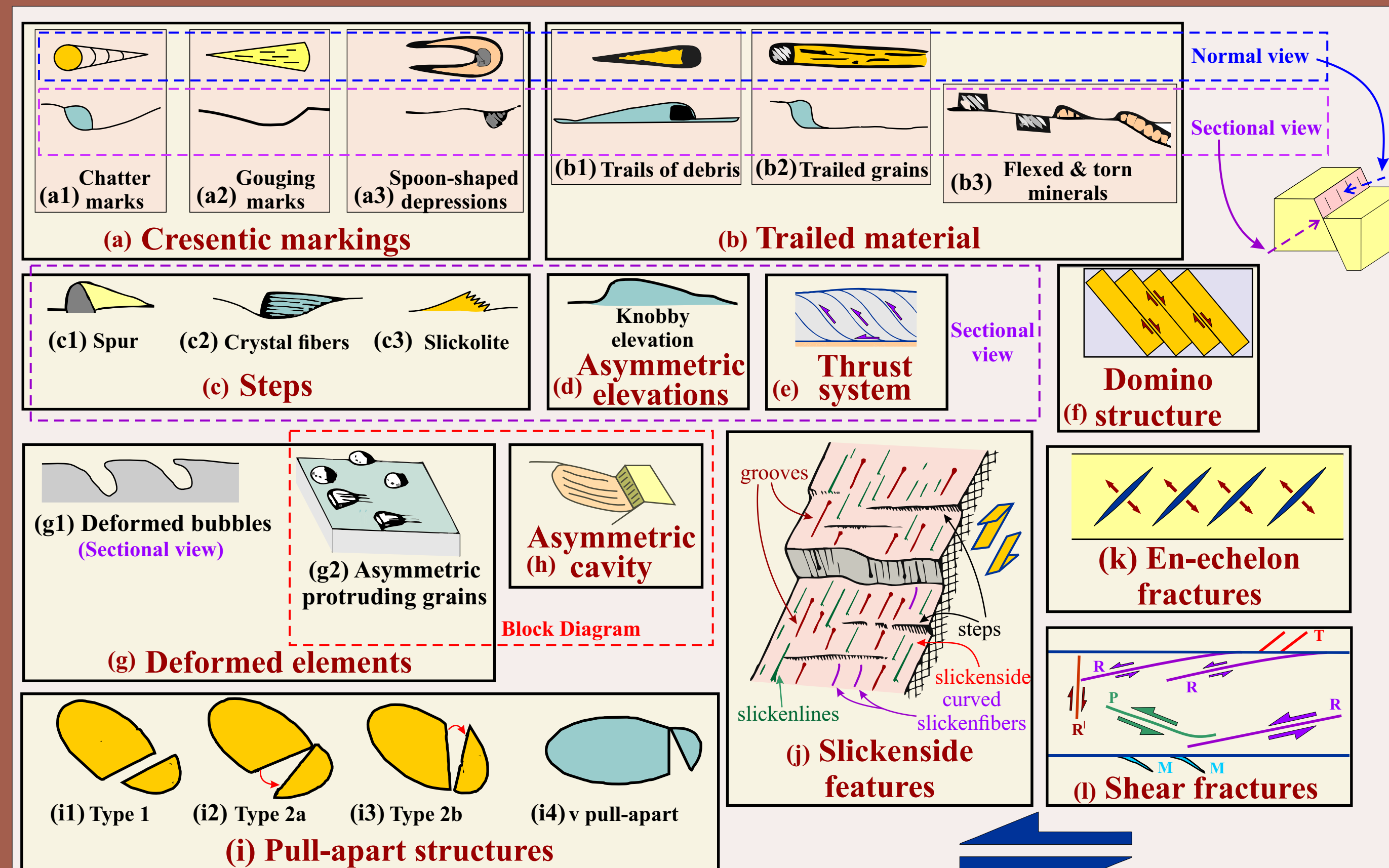


Fig. 2. Major brittle shear sense indicators observed at different scales. Reproduced from (a,b,c,d,g,h) fig. 1 of Doblas (1998), (i1, i2, i3) fig. 4 of Samanta et al. (2002), (i4) fig. 1 of Hippertt (1993), (j) fig. 3 of Tjia (1964), fig. 6 of Twiss & Gefell (1990), (l) fig. 1c of Petit (1987), fig. 5.50 of Passchier & Trouw (2005). Shear sense: sinistral (blue half-arrows) except for (j) for which the relative sense of movement of the blocks have been denoted separately.

4. Geneses

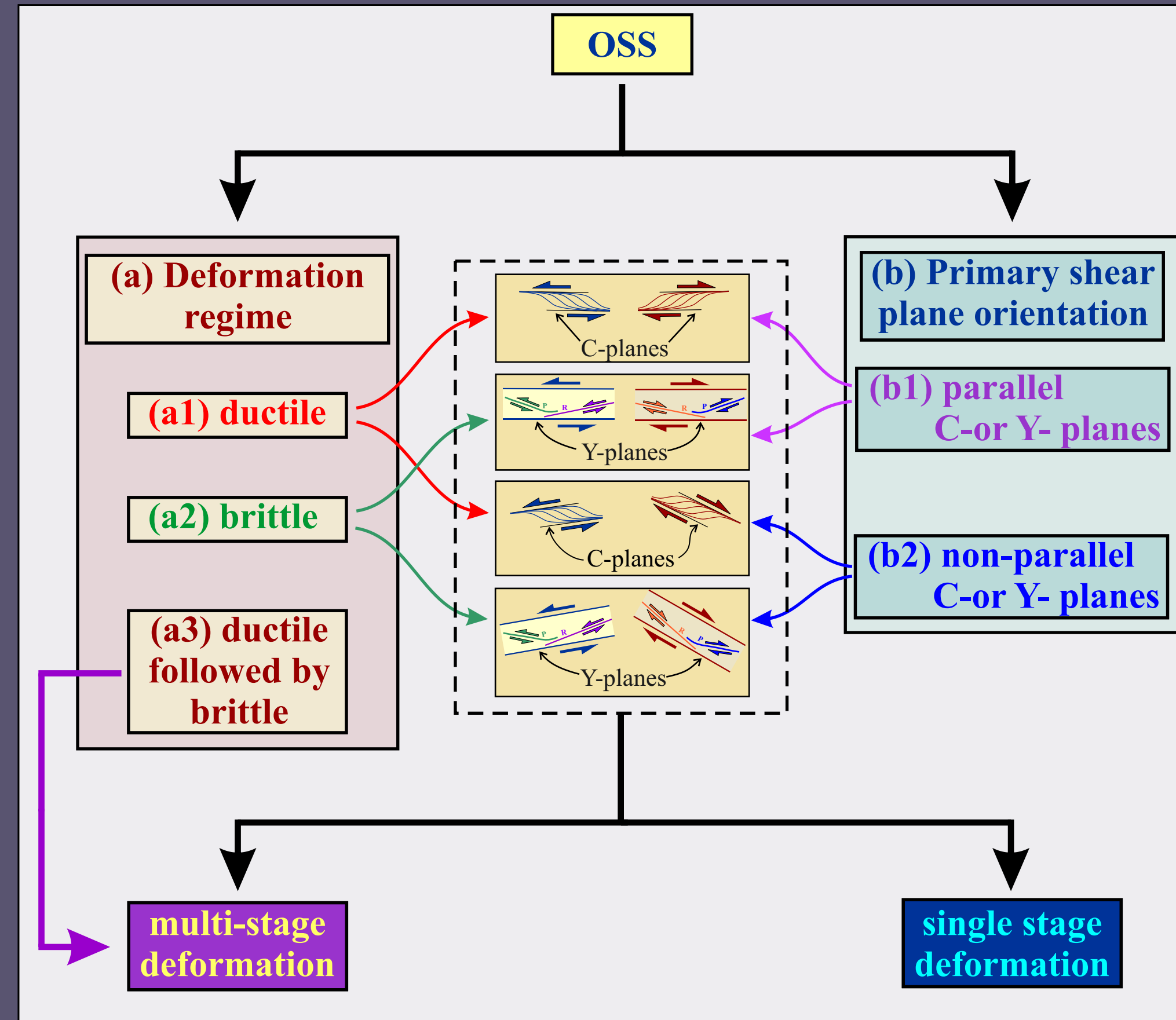


Fig. 3. Flowchart depicting the categorization of OSS based on deformation regime and orientation of the primary shear planes.

5. Single-stage deformation

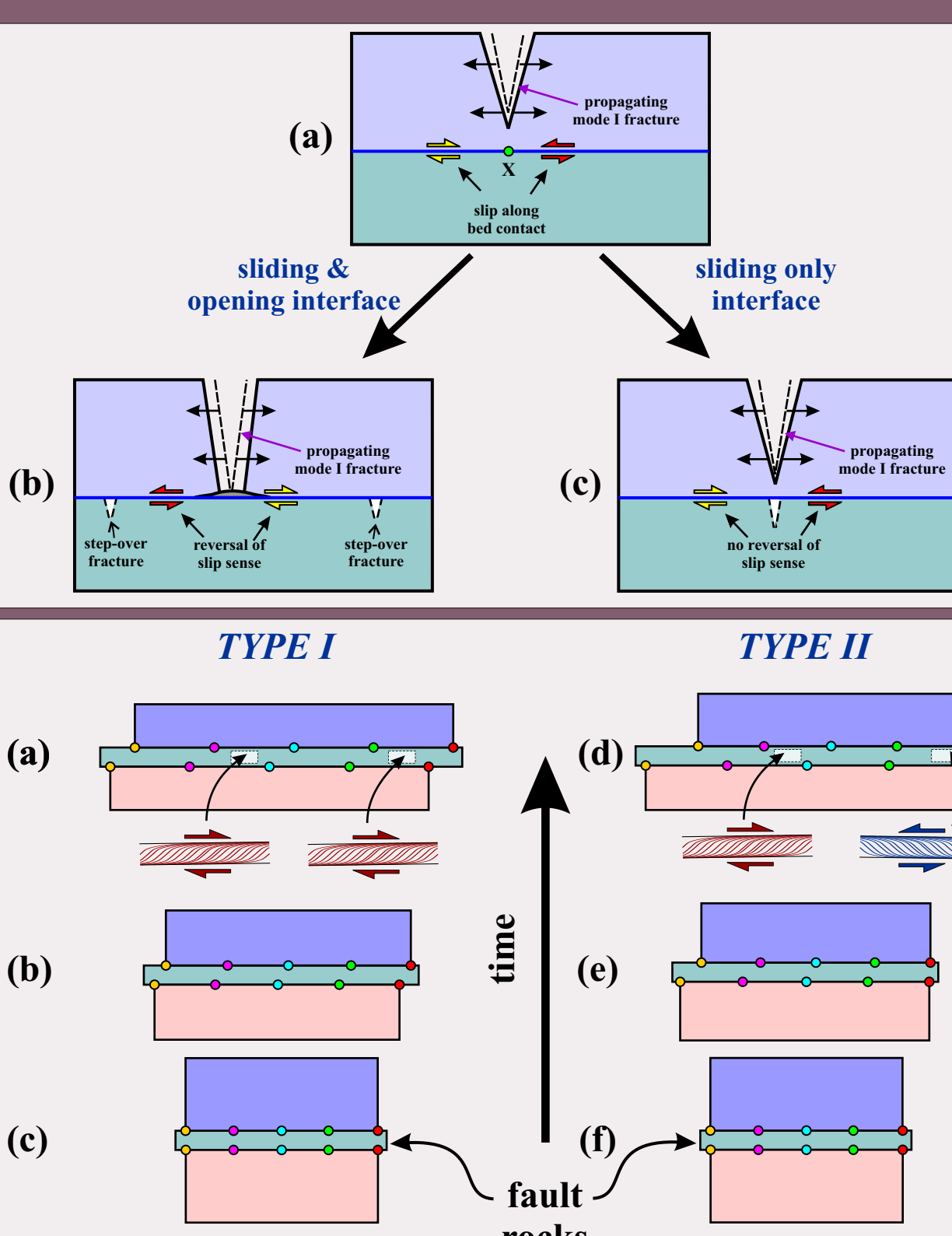


Fig. 4. Results of the two numerical experiments showing interaction between fracture propagation and the bedding interface of moderate strength. (a) The fracture tip is ~ 3 cm away from the contact. Shear sense reversal at the bed contact. (b) Both sliding and opening along the contact; shear sense reversal due to step-over fractures. (c) Only sliding, fractures migrate across the contact. Unlike (b), no shear reversal occurs. Reproduced from figs. 9 & 11e of Cooke & Underwood (2001).

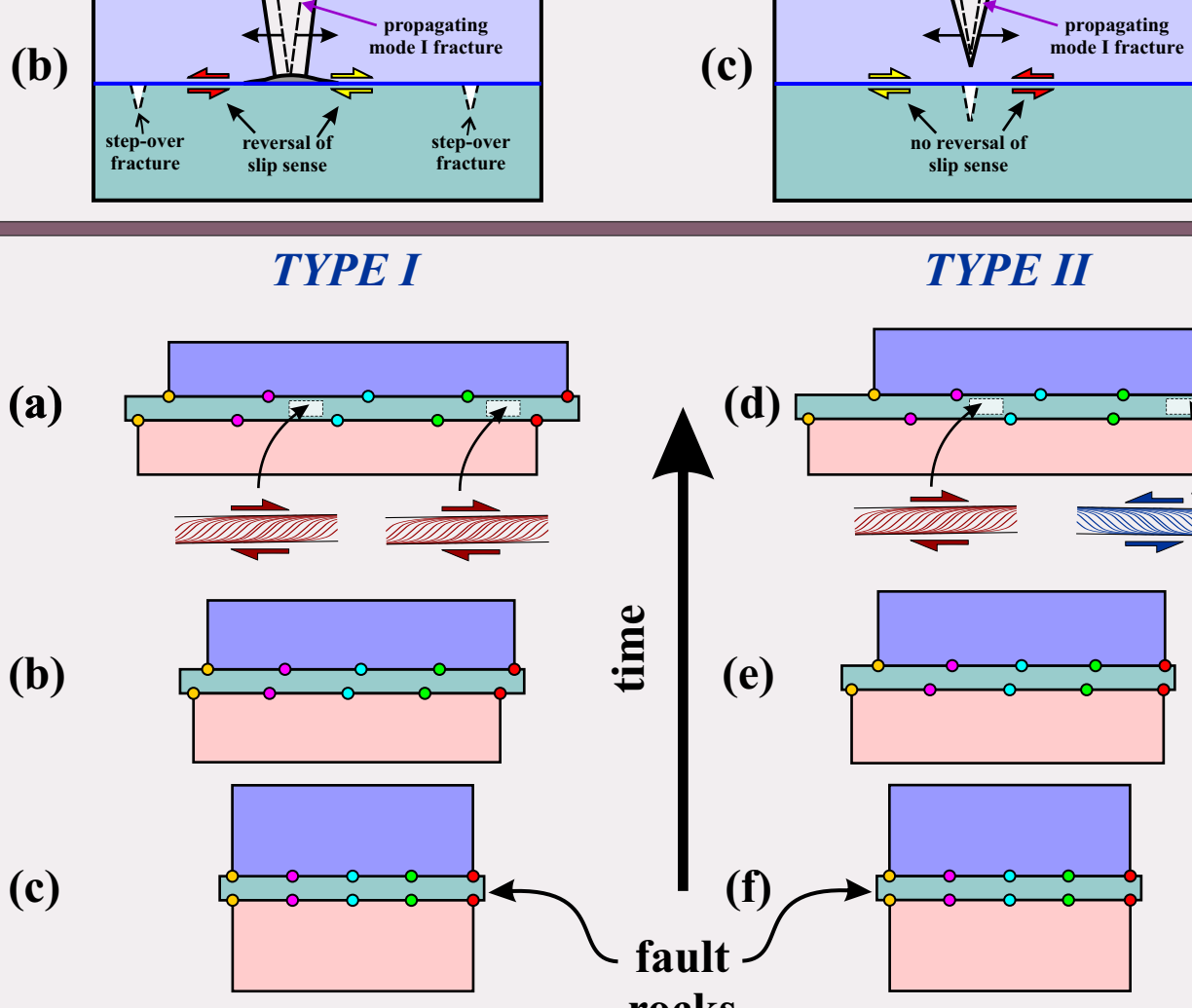


Fig. 5. Results of the 2D numerical experiments performed by Ishii (1992). OSS due to viscosity inhomogeneity. (a) Type I. No shear reversal along the shear zone (d,e,f). Type II. Shear reversal along the shear zone. After Means (1990).

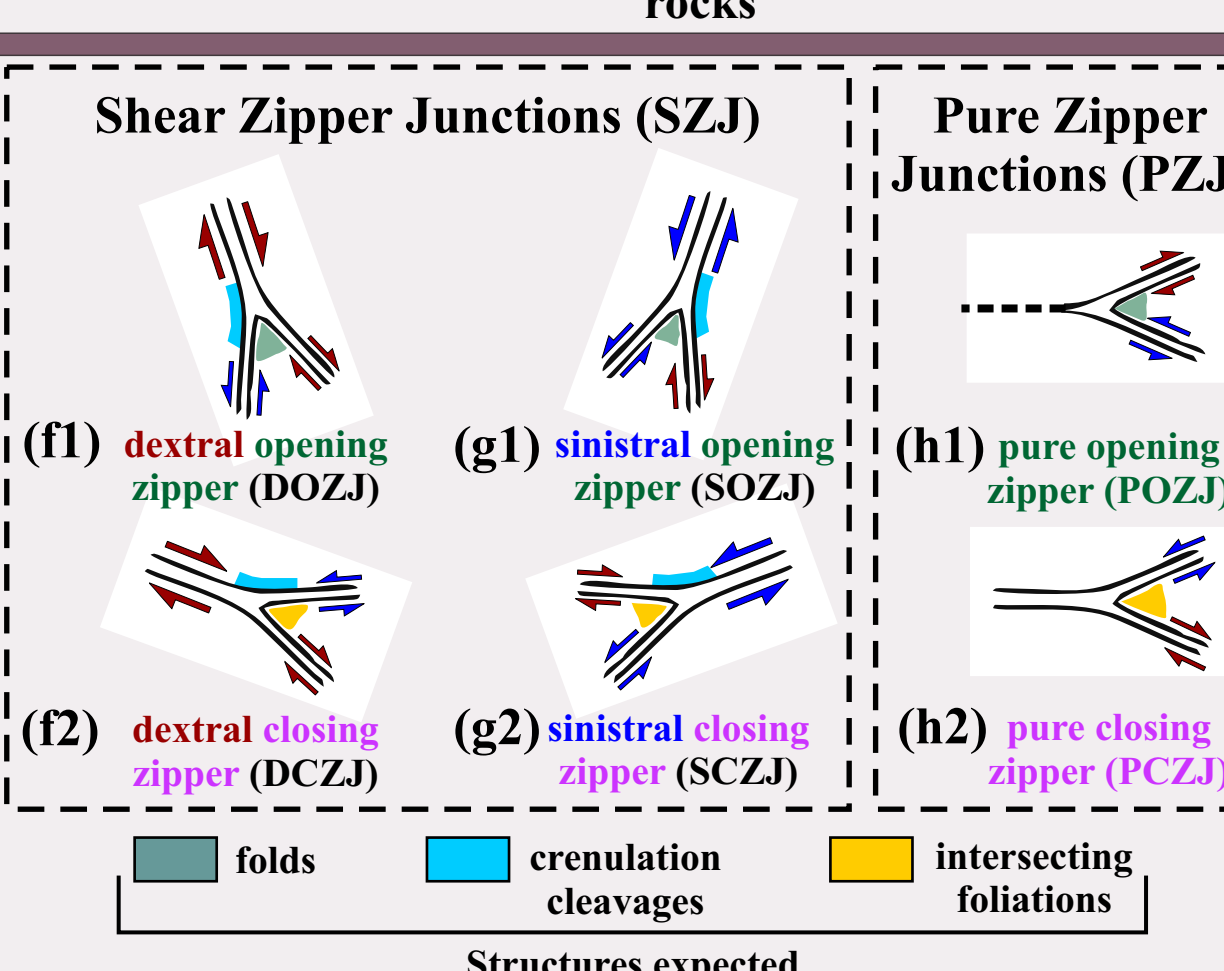


Fig. 6. Stretching faults. (a,b,c) Type I. No shear reversal along the shear zone (d,e,f). Type II. Shear reversal along the shear zone. After Means (1990).

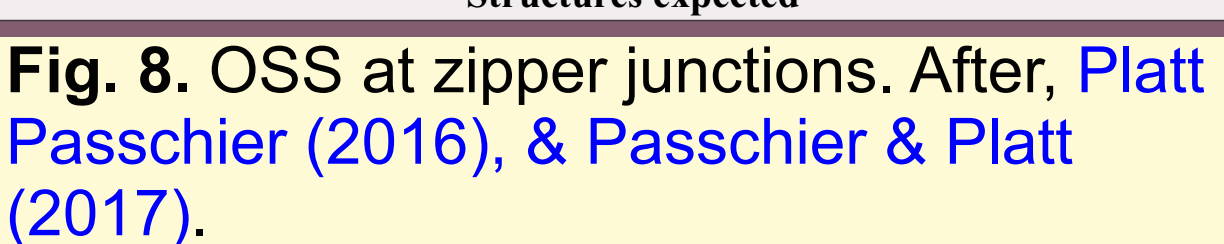


Fig. 7. OSS in a multi-layered rock. (a-c) Anhydrous condition. Active layer (quartz-rich) deforms more than passive (feldspar-rich) one. (d-f) Hydrated condition. Passive becomes active (e.g. feldspar -> muscovite) and vice-versa (quartz is stronger than muscovite). OSS develop at domain boundaries in both. After, Hippertt & Tohver (1999).



Fig. 8. OSS at zipper junctions. After, Platt & Passchier (2016), & Passchier & Platt (2017).

6. Multi-stage deformation

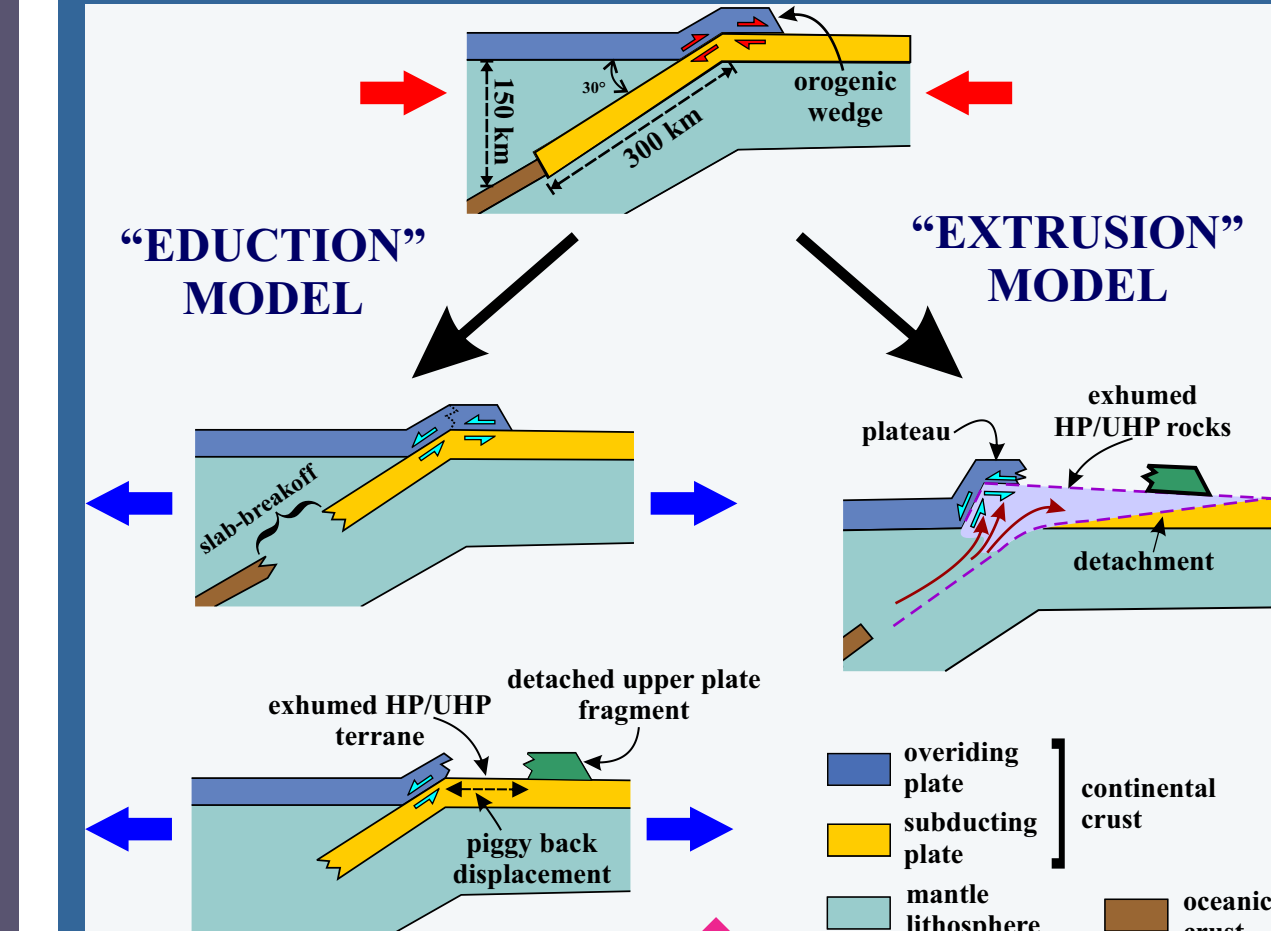


Fig. 9. OSS in exhumed terranes. After, Brueckner & Cuthbert (2013).

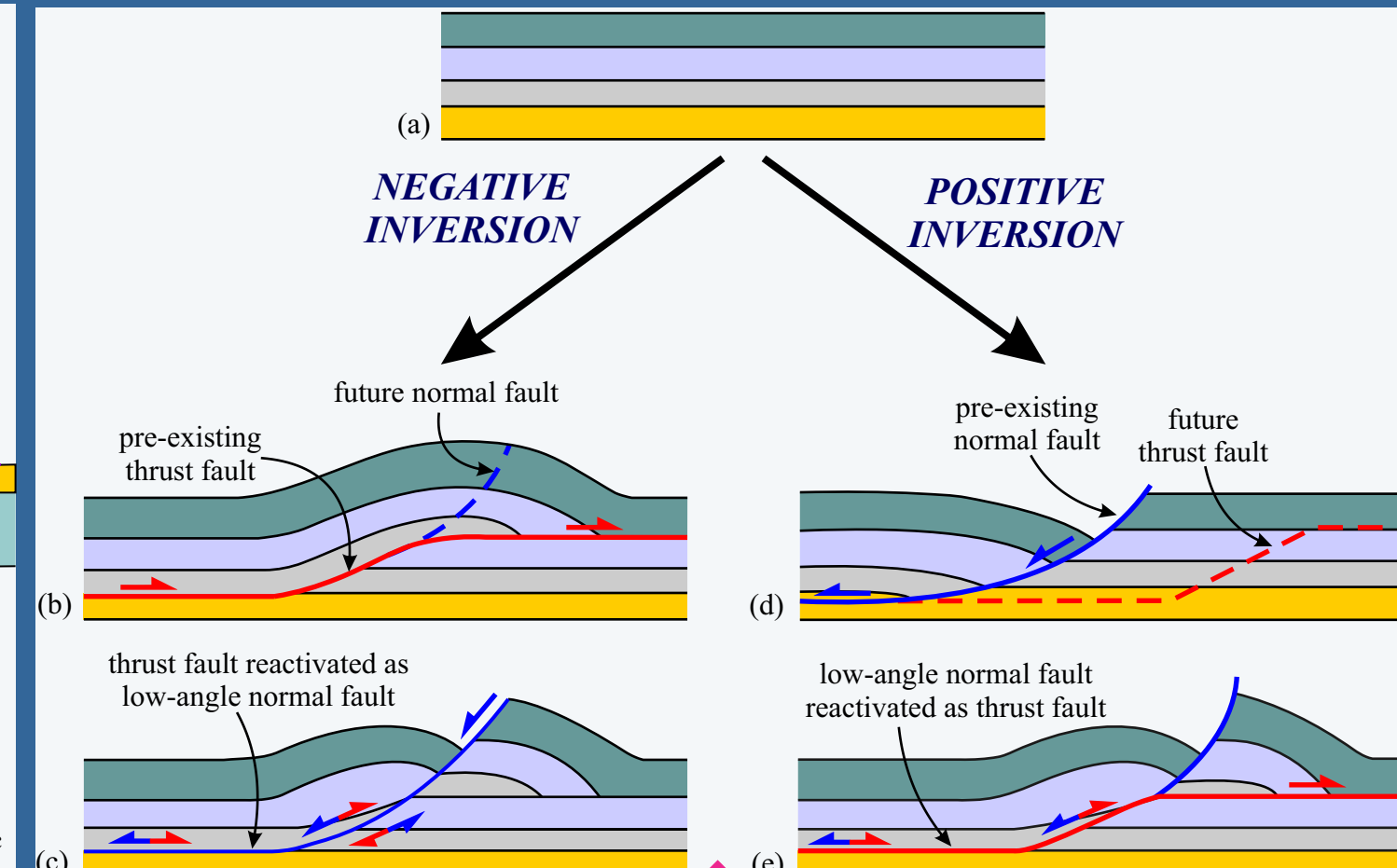


Fig. 10. Inversion tectonics in a sedimentary basin. (a) Sequence of beds after deposition. Two headed half-arrows indicate zones where evidences of both contraction and extension can be found (b,c) negative, (d,e) positive. After, Tavarnelli (1999).

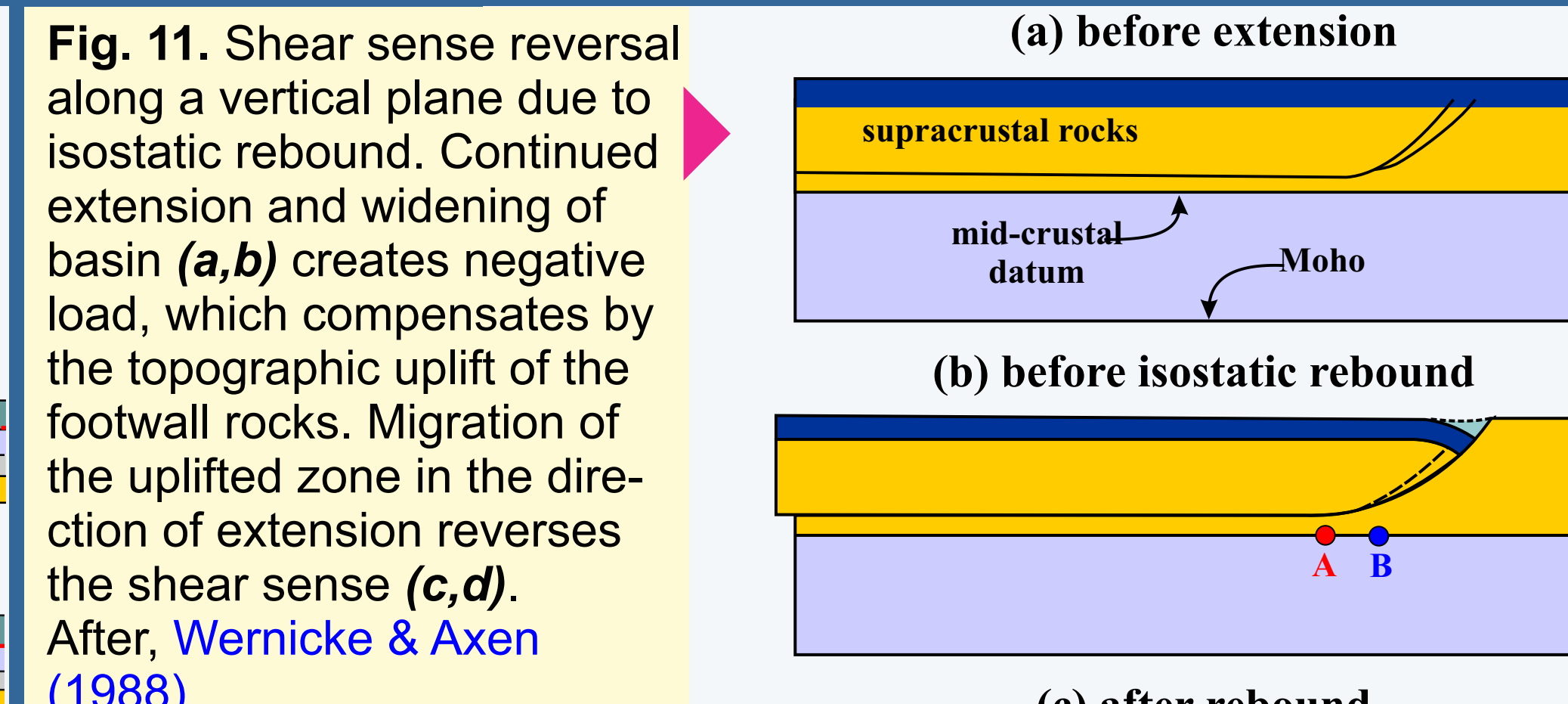


Fig. 11. Shear sense reversal along a vertical plane due to isostatic rebound. Continued extension and widening of basin (a,b) creates negative load, which compensates by the topographic uplift of the footwall rocks. Migration of the uplifted zone in the direction of extension reverses the shear sense (c,d). After, Wernicke & Axen (1988).

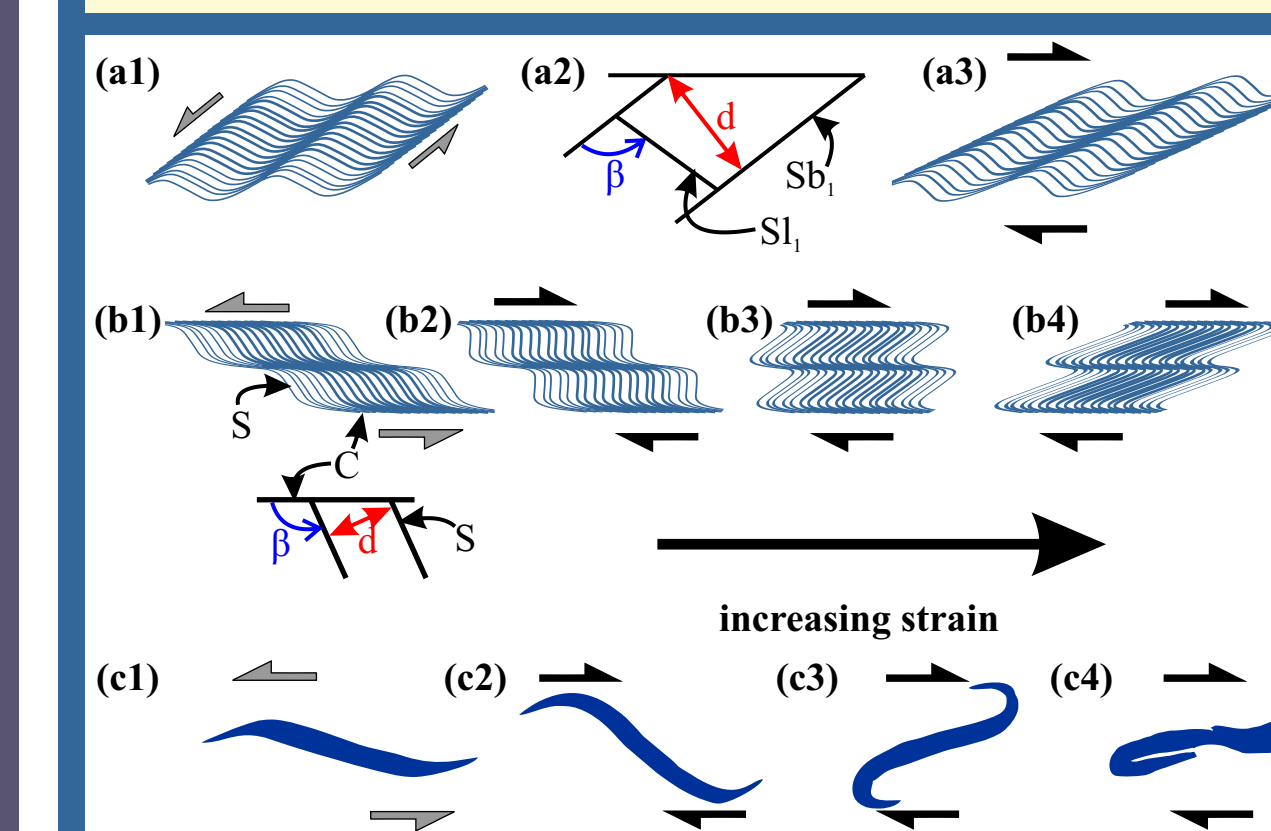


Fig. 12. Overprinting (sinistral shear followed by dextral shear) of deformations & variations in the morphologies of (a1-a3, b1-b4) shear bands, & (c1-c4) isolated vein. After, Wennberg (1996).

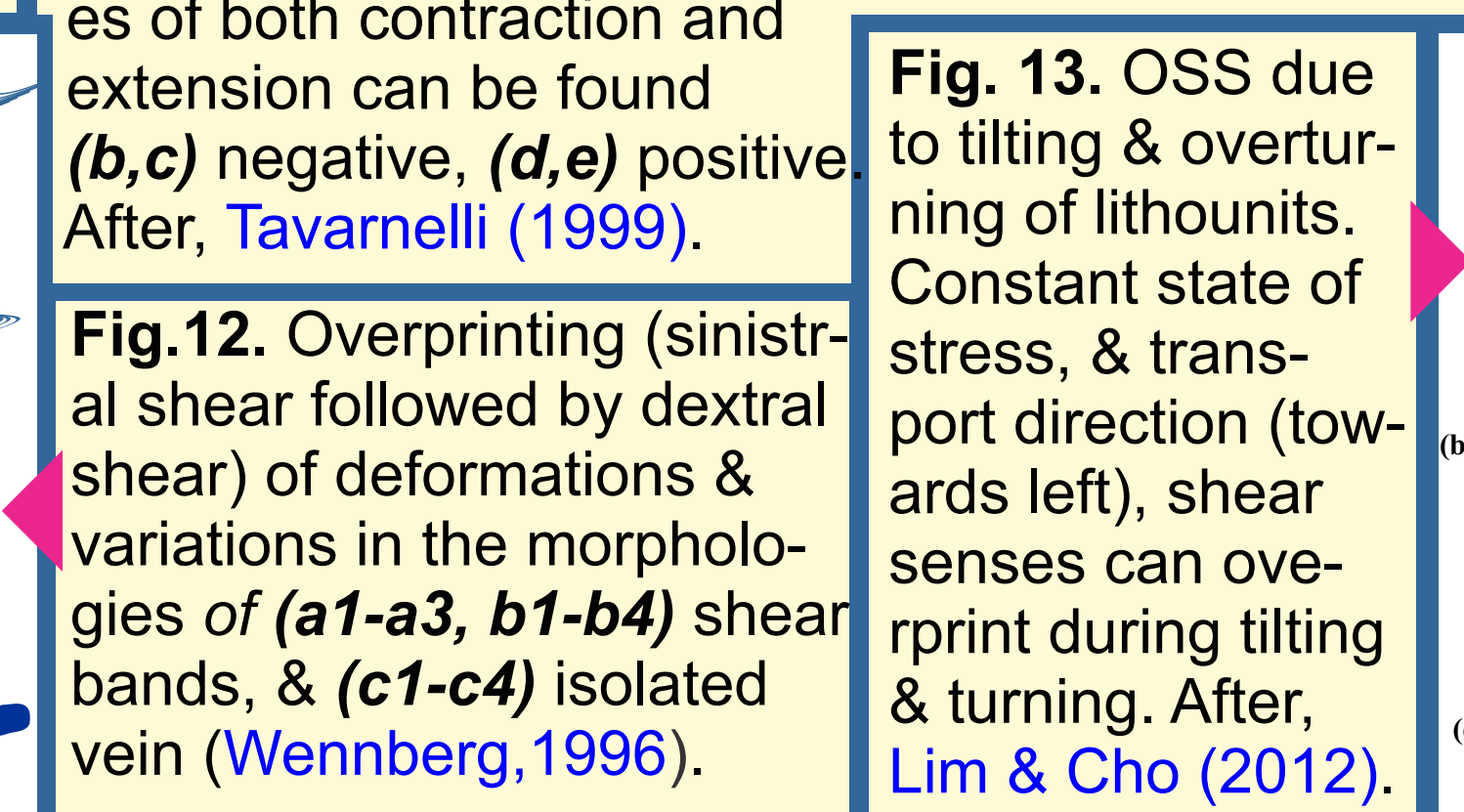


Fig. 13. OSS due to tilting & overturning of lithounits. Constant state of stress, & transport direction (towards left), shear senses can overprint during tilting & turning. After, Lim & Cho (2012).

7. Global reports



Fig. 14. Global distribution of OSS reported in the literature.

8. Case study: Sutlej river section, India

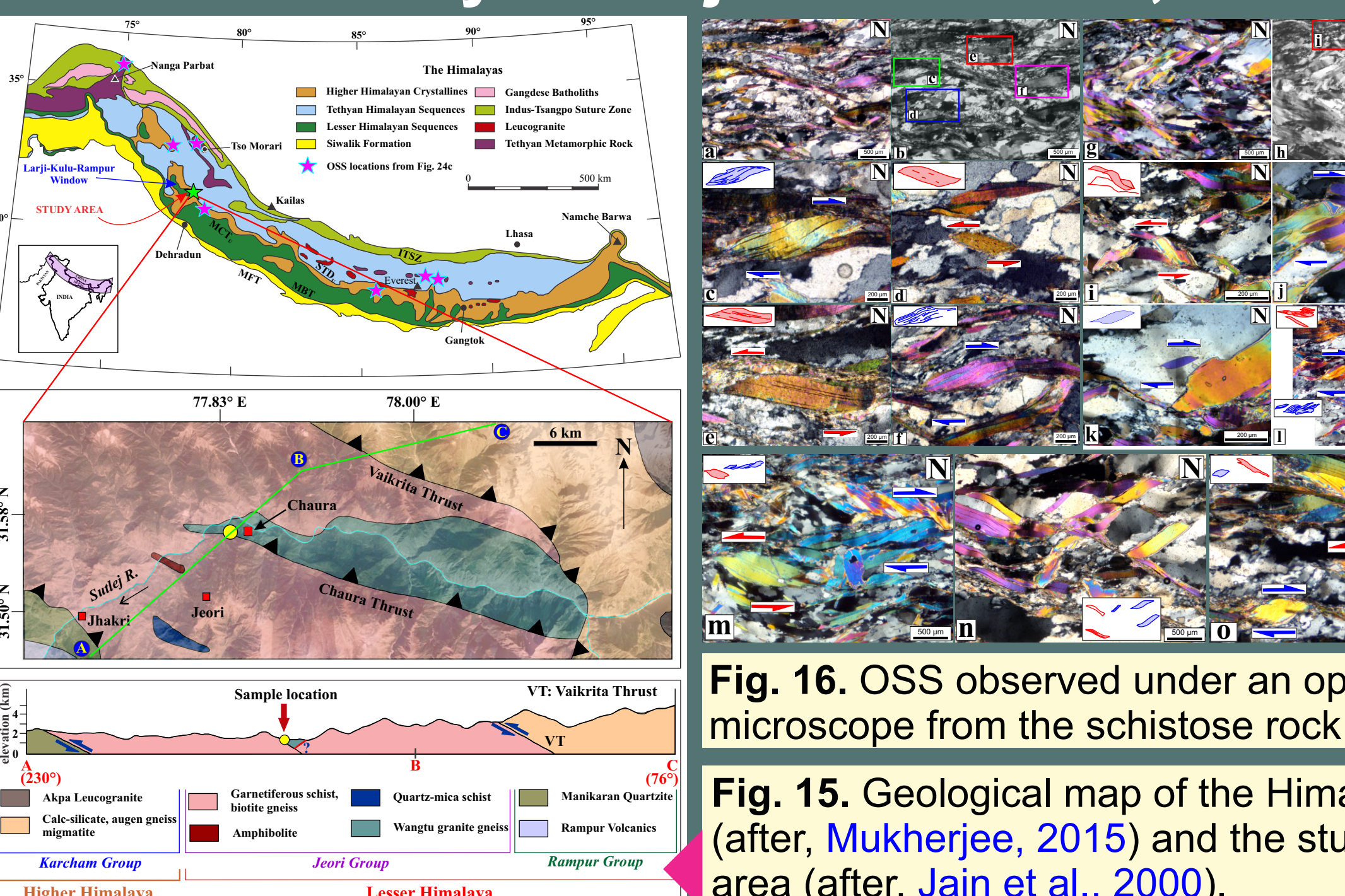


Fig. 15. Geological map of the Himalaya (after, Mukherjee, 2015) and the study area (after, Jain et al., 2000).

9. Discussions & Conclusions

- ▶ OSS is present in many shear zones across the globe, especially at **orogenic belts**. 16 locations belong to Precambrian cratonic shields. However, proper cautions must be exercised in their identification to avoid misinterpretations.
- ▶ Multiply deformed terranes, which have undergone orthogonal switching of the principal stress axes (both local and/or regional), are more likely to exhibit OSS. However, they are yet to be reported from the **Zagros** & the **Andes**.
- ▶ It is noticed that OSS in **fold-thrust belts** are mostly results of either gravitational collapse (e.g. **Nepal Himalaya**, **North American Cordillera**) or reorientation of principal stress axes (e.g. **Apennines**, **Eastern Alps**)
- ▶ Tectonic inversion, a major cause of producing OSS, of sedimentary basins play a crucial part in **hydrocarbon prospectivity**. Hence, structural evolution of basins should be vigorously studied with special emphasis on identification of OSS.
- ▶ The equal abundance of OSS in the mylonitic sample from the Higher Himalayan Crystallines (HHC) suggests dominance of coaxial deformation, which has been previously reported from different portions of the HHC.